Journal of Medicinal Chemistry

Article

6-Amino-3-Methylpyrimidinones as Potent, Selective, and Orally Efficacious SHP2 Inhibitors

Patrick Sarver, Michael G Acker, Jeffrey Bagdanoff, Zhuoliang Chen, Ying-Nan P Chen, Homan Chan, Brant Firestone, Michelle Fodor, Jorge Fortanet, Huaixiang Hao, Murphy Hentemann, Mitsunori Kato, Robert Koenig, Laura R. LaBonte, Gang Liu, Shumei Liu, Chen Liu, Eric McNeill, Morvarid Mohseni, Martin Sendzik, Travis Stams, Stan Spence, Victoriano Tamez, Ritesh Tichkule, Christopher S. Towler, Hongyun Wang, Ping Wang, Sarah L. Williams, Bing Yu, and Matthew J. LaMarche

J. Med. Chem., **Just Accepted Manuscript** • DOI: 10.1021/acs.jmedchem.8b01726 • Publication Date (Web): 28 Jan 2019

Just Accepted

ACS Publications

is published by the American Chemical Society. 1155 Sixteenth Street N.W., Washington, DC 20036

	LaMarche, Matthew; Novartis Institutes for BioMedical Research Inc, Oncology Medicinal Chemistry

6-Amino-3-Methylpyrimidinones as Potent, Selective, and Orally Efficacious SHP2 Inhibitors

*Patrick Sarver,[a] Michael Acker,[b] Jeffrey T. Bagdanoff,[a] Zhouliang Chen,[a] Ying-Nan Chen,[b] Homan Chan,[b] Brant Firestone,[b] Michelle Fodor,[c] Jorge Fortanet,[a] Huaixiang Hao,[b] Murphy Hentemann,[b] Mitsunori Kato,[a] Robert Koenig,[a] Laura R. LaBonte,[d] Gang Liu,[a] Shumei Liu,[b] Chen Liu,[b] Eric McNeill,[a] Morvarid Mohseni,[b] Martin Sendzik,[a] Travis Stams,[c] Stan Spence,[b] Victoriano Tamez,[a] Ritesh Tichkule,[a] Christopher Towler,[e] Hongyun Wang,[b] Ping Wang,[b] Sarah L. Williams,[a] Bing Yu,[a] and Matthew J. LaMarche[a]**

[a]Global Discovery Chemistry, [b]Oncology Disease Area, [c]Chemical Biology & Therapeutics, [d]Pharmacokinetic Sciences, Novartis Institutes for Biomedical Research, and [e]Chemical and Pharmaceutical Profiling, Novartis Pharmaceuticals, 250 Massachusetts Avenue, Cambridge, Massachusetts, 02139, United States

ABSTRACT

Protein tyrosine phosphatase SHP2 is an oncoprotein associated with cancer as well as a potential immune modulator due to its role in the programmed cell death PD-L1/PD-1 pathway. In the preceding manuscript, we described the optimization of a fused, bicyclic screening hit for

potency, selectivity, and physicochemical properties in order to further expand the chemical diversity of allosteric SHP2 inhibitors. In this second manuscript, we describe the further expansion of our approach, morphing the fused, bicyclic system into a novel monocyclic pyrimidinone scaffold through our understanding of SAR and use of structure-based design. These studies led to the identification of SHP394 (**1**), an orally efficacious inhibitor of SHP2, with high lipophilic efficiency, improved potency and enhanced pharmacokinetic properties. We also report other pyrimidinone analogs with favorable pharmacokinetic and potency profiles. Overall, this work improves upon our previously described allosteric inhibitors, and exemplifies and extends the range of permissible chemical templates that inhibit SHP2 via the allosteric mechanism.

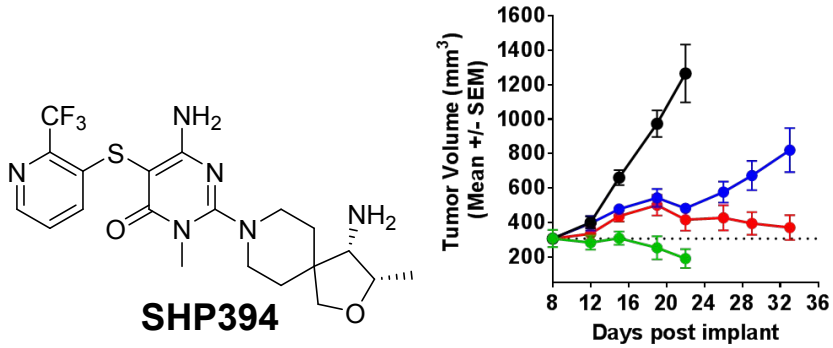

INTRODUCTION

Mutations in the *Ptpn11* gene, which encodes the non-receptor protein tyrosine phosphatase (PTP) SHP2, are associated with several human diseases. Hyperactivating mutations of SHP2 has been observed in Noonan syndrome (50%),[1] juvenile myelomonocytic leukemia (JMML, 35%), myelodysplastic syndrome (10%), B-cell accute lymphoblastic leukemia (7%), acute myeloid leukemia (AML, 4%),[2] and a number of solid tumors.[3] Although its precise role is not fully understood, SHP2 functions in the cytoplasm downstream of various receptor-tyrosine kinases and is involved in oncogenic cell signaling cascades including RAS-ERK, PI3K-AKT, and JAK-STAT.[4] SHP2 may also play a role in the PD-L1/PD-1 pathway, suggesting possible

applications of SHP2 inhibition in immuno-oncology.[5,6] Given the demonstrated importance of SHP2 to human diseases, small molecule inhibition of SHP2 has attracted significant attention in the scientific community.[7] Over the last two decades, a number of small molecule active site inhibitors have been described, but have not progressed to the clinic.[8] Due to the challenges inherent to targeting the active site of phosphatases,[9] for example the inherent polarity and difficulty in achieving selectivity across the phosphatome, the general concept of allosteric phosphatase inhibition is gaining momentum.[10]

Previously, we reported a screening method that led to the identification of a new site for allosteric SHP2 inhibition.[11] Initial medicinal chemistry efforts identified a moderately potent, selective, and orally bioavailable inhibitor, SHP099 (**2**, Figure 1a).[12] By concurrently binding to the interface of the N-terminal SH2, C-terminal SH2, and protein tyrosine phosphatase domains, **2** stabilizes an inactive conformation in which the active site is inaccessible to substrates. This binding modality resembles the published inactive apo structure (PDB code 2SHP), [13] in which the *N*-terminal SH2 domain blocks the active site, resulting in autoinhibition of PTP activity.

During the course of the discovery and characterization of **2** (Figure 1A), we sought to investigate other chemical matter which would provide structural and property diversification. Part of this effort to generate new chemotypes focused on alternative screening strategies. We[14] and others[15] employed oncogenic mutants of SHP2. We also engineered inhibitor-resistant mutants to identify an additional allosteric site for SHP2 inhibition,[16] and then demonstrated that dual allosteric inhibition of SHP2 was possible. In the preceding paper,[17] multiple, unique, fused-bicyclic screening hits were optimized for potency, selectivity and structural diversity. These studies identified potent and selective inhibitors that are structurally distinct from **2**. Additionally, this work further explored the allosteric pocket, identifying important elements of the

pharmacophore such as a thioether functionality, and the conformationally restricted spirocyclic amine motif.

Despite the successful optimization for potency and selectivity of this fused-bicyclic template, it remained difficult to identify pyrazolo-pyrimidinones, or related fused systems, which coupled these properties with acceptable oral exposure and ADME properties. In order to further broaden our approach to SHP2 allosteric inhibition and access more desireable ADME and property space, we employed a scaffold-morphing strategy using the pyrazolo-pyrimidinones as a starting point. This exploited our working knowledge of the SAR, a compendium of HTS data, and structure-based design. In this, the second of two papers, we report the discovery of 6-amino-3-methylpyrimidinones as potent, selective, and orally efficacious SHP2 inhibitors with favorable physicochemical and ADME properties.

RESULTS AND DISCUSSION

As in our previous studies, we utilized a well-precedented, fluoresence-based phosphatase biochemical assay measuring dephosphorylation of 6,8-difluoro-4-methylumbelliferyl phosphate (0.5 μM 2P-IRS-1, DIFMUP assay[18]). We also evaluated modulation of p-ERK and DUSP6 as downstream markers of MAPK pathway activity, and antiproliferation activity in the EGFR amplified human esophageal squamous cell carcinoma cell line KYSE520 and in Detroit-562, a pharyngeal carcinoma cell line. Early investigations of the pyrazolo-pyrimidinone scaffold (see preceding paper) for SHP2 inhibition led to the identification of **3** (Figure 1A), a 5,6-fused system bearing the same aryl and aminopiperidine present in **2**. Comparison of the X-ray binding poses of **3** and aminopyrazine **2** (PDB codes *6MDB*, *5EHR* respectively; overlay in Figure 1B) indicated significant overlap of the six-membered pyrimidinone ring and the aminopyrazine. Several interactions of **3** with the protein are quite similar to those previously described for **2**:[12] the

pyrimidinone carbonyl of **3** makes a crucial hydrogen bond with R111, positioning the residue for *Pi*-cation stacking interaction with the dichlorophenyl motif; the dichlorophenyl occupies a hydrophobic area of the pharmacophore (e.g., L254, Q257, P491); the pyrazole forms a hydrogen bond with E250; the primary amine makes contacts with the backbone carbonyl of F113. Given the challenges in identifying compounds from the pyrazolo-pyrimidinones with an acceptable balance of potency, hERG selectivity, and oral exposure (see preceding paper), we redirected our efforts towards monocyclic central ring systems in an effort to ease multiparameter optimization. Thus, breaking the 5-6 ring fusion by removal of the pyrazole ring in **3** and joining the dichlorophenyl directly to the pyrimidinone resulted in **4** (Figure 1A). Compound **4** is equipotent to **2** and **3** in the biochemical assay (IC_{50} = 0.105 μM). Importantly, as reduced lipophilicity is strongly correlated with improved in vivo properties,[19] the monocyclic pyrimidinone has lower lipophilicity (cLogP = 1.9) and increased lipophilic efficiency (5.1).

A.

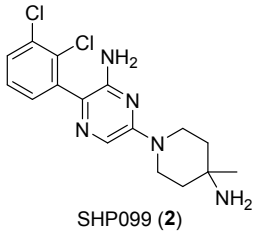

SHP099 (**2**)

SHP2 IC_{50} = 0.071 μM
p-ERK IC_{50} = 0.250 μM
antiprolif. IC_{50} = 1.4 μM
cLogP = 3.0, LipE = 4.5

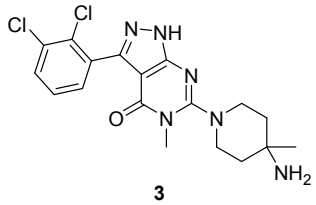

3

SHP2 IC_{50} = 0.067 μM
p-ERK IC_{50} = 0.746 μM
antiprolif. IC_{50} = 4.8 μM
cLogP = 2.4, LipE = 4.9

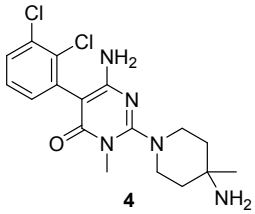

4

SHP2 IC_{50} = 0.105 μM
p-ERK IC_{50} = ND
antiprolif. IC_{50} = ND
cLogP = 1.9, LipE = 5.1

B.

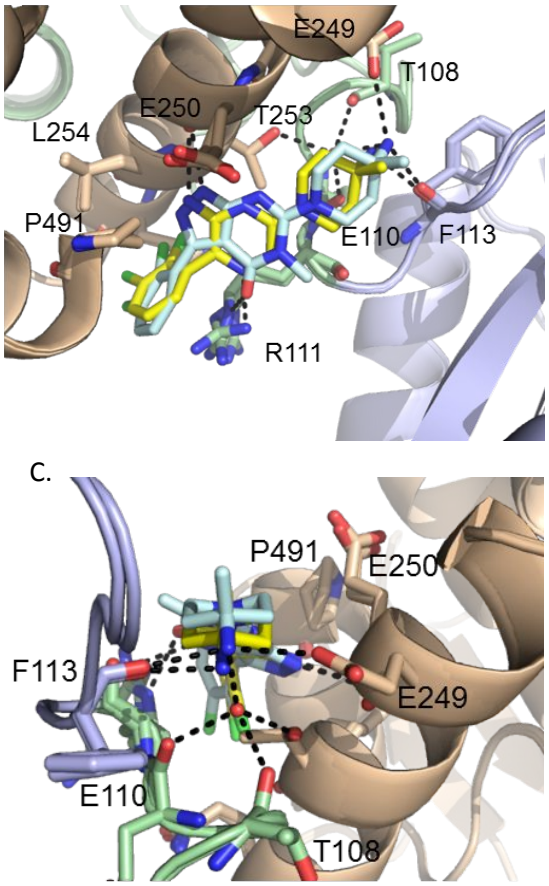

Figure 1. A. Design of pyrimidinones **4** from pyrazine (**2**) and pyrazolo-pyrimidinone (**3**). B. Overlay of X-ray of **2**-SHP2 (PDB code 5EHR) and **3**-SHP2 (PDB code *6MDB*) in the allosteric binding pocket of SHP2. C. Amine region overlay: X-ray of **2**-SHP2 and **3**-SHP2.

The fused bicycle of **3** is also reminiscent of another screening hit, azabenzimidazole **5** (Figure 2A), a weak inhibitor of SHP2 (IC_{50} = 46 μM) that also interacts with R111 via the pyridine N, thereby preorganizing the dichlorophenyl ring into the hydrophobic cleft and towards a *Pi*-cation interaction with R111 in a similar fashion to **2** and **3**. Notably, **5** and **3** both join the dihalo-arene with the central ring by the same number of atoms, yet with different functional groups: a thioether vs. a pyrazole ring, respectively. With the removal of the pyrazole ring in **4**, we hypothesized that the thioether linker from **5** would successfully replace and mimic the pyrazole

and also balance the substantially increased polarity of the central pyrimidinone ring. In addition, our SAR understanding of the allosteric binding pocket allowed us to also consider amine extension. In previous studies (see preceding paper), homologation of the amine displaced a structural water allowing for binding interactions directly to the protein (Figure 1C and *vide infra*). We thus incorporated the thioether linker and amine extension into our monocyclic pyrimidinone design, which resulted in **6**. We evaluated **6** in the biochemical and cellular assays and found improved biochemical potency (IC_{50} = 0.012 μM) relative to the aminopyrazine, pyrazolo-pyrimidinone, and aminopyrimidinone starting points (**2**: IC_{50}= 0.071 μM; **3**: IC_{50}= 0.064 μM; **4**: IC_{50}= 0.105 μM, respectively), as well as improved cellular potency (**6**: p-ERK IC_{50} = 0.049 μM, antiproliferation IC_{50} = 0.273 μM). Compound **6** was also evaluated for solubility in aqueous buffer (0.25 mM at pH 6.8), permeability (Caco-2: 2.5 x 10^{-6} cm/s),[20] and hERG activity (IC_{50} = 6 μM). Taken together, these results indicated that the pyrimidinone template was an attractive starting point for further optimization (e.g., potency, permeability, hERG selectivity). We were further encouraged by the presence of the 4-pyrimidinone moiety in a range of marketed and developmental drugs.[21]

A.

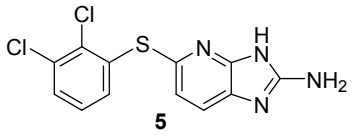

5

SHP2 IC_{50} = 46 μM
cLogP = 4.8
LipE = 2.7

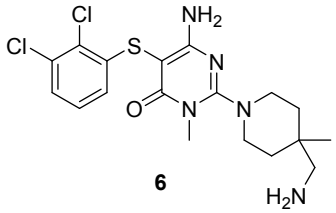

6

SHP2 IC_{50} = 0.012 μM
p-ERK IC_{50} = 0.049 μM
antiprolif. IC_{50} = 0.273 μM
cLogP = 3.2, LipE = 4.9

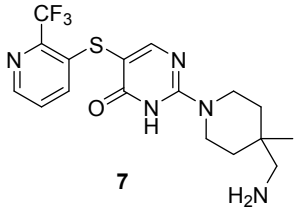

7

SHP2 IC_{50} = 0.181 μM
p-ERK IC_{50} > 2.0 μM
antiprolif. IC_{50} > 2.0 μM
cLogP = 3.2, LipE = 3.6

B.

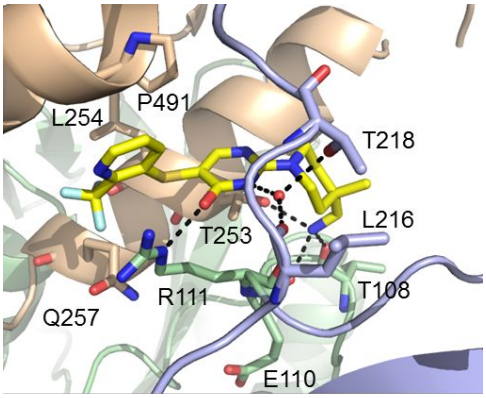

Figure 2. A. Thioether-azabenzimidazole HTS hit **5** and thioether-pyrimidinones **6** and **7**. B. X-ray of **7** and SHP2 (PDB code *6MD7*).

Our optimization was facilitated by X-ray crystallography of a less potent analog (Figure 2A: **7**, IC_{50} = 0.181 μM) bound to SHP2 (PDB code *6MD7*) in a conformation resembling the

bound aminopyrazines and pyrazolopyrimidinones (Figure 2B). As anticipated, the central pyrimidinone ring of **7** occupies a position nearly identical to that of the 5,6-fused pyrimidinone in **3** and the aminopyrazine in **2**. Further comparison of the binding pose of **7** and **2** indicated that the aminopyrazine of **2**, which was previously shown to engage in hydrogen bonding with backbone carbonyl of E250 and substantially improve potency, could likely be reintroduced at the 6-position of the pyrimidinone (*vide infra*). The crystal structure of **7**-SHP2 also revealed that the pyrimidinone oxygen facilitates a *Pi*-cation interaction with R111 and the trifluoromethyl-pyridine, through a hydrogen bond interaction. This resembles a similar *Pi*-cation interaction preorganized by the pyrazine nitrogen of **2**, despite a distance of one bond length between the pyrimidinone oxygen and pyrazine nitrogen. In addition, the extended amine in **7** displaced a structural water found in the X-ray of 2-SHP2 (PDB code 5EHR), making direct interactions with several residues (e.g., T253, S109, E110). Importantly, **7** was selective over the hERG channel (IC_{50} > 30 μM), indicating that increasing the polarity of the central scaffold could result in higher hERG selectivity. The overlay of **7** and other scaffolds (i.e., **2**, **3**: not shown) also showed excellent overlap of the aryl and amine regions, suggesting that previously developed SAR could be transferrable from the aminopyrazines and pyrazolopyrimidinones to the monocyclic pyrimidinones. This enabled the application of a range of previously investigated fragments in our continued efforts to optimize this novel template.

Given the polar core present in the aminopyrimidinones, we hypothesized that re-optimization of the aryl thioether and spirocyclic amine could yield significant improvements in balancing potency, permeability, and oral exposure. First, we utilized a spiro[4.5]-furanyl-amine moiety (e.g., **8**, Table 1) which had proven to improve potency and permeability, and reduce the pKa of the basic amine in other scaffolds (see preceding paper). Compound **8** exhibited 4 to 10-

fold improvement compared to **6** in the cellular assays (p-ERK IC_{50} = 0.005 μM, antiproliferation IC_{50} = 0.069 μM) and acceptable oral exposure (dose-normalized to 1 mg/kg PO, 0.95 μM·h) and bioavailability (38 %*F*) in rat.

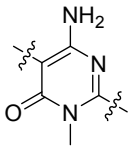

compound	Ar-	amine	*SHP2 IC_{50} (μM)*	*p-ERK IC_{50} (μM)*	*antiproliferation IC_{50} (μM)*	*cLogP/LipE*	*hERG IC_{50} (μM)*
6	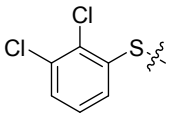	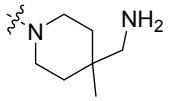	0.012	0.049	0.273	3.2/4.9	6.0
8	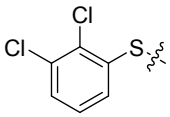	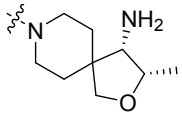	0.005	0.005	0.069	3.0/5.8	4.0
9	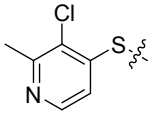	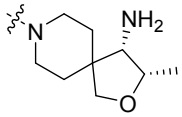	0.048	0.028	0.220	1.5/6.0	>30
10	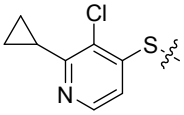	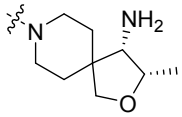	0.014	0.010	0.295	2.0/6.0	9.8
1	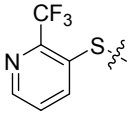	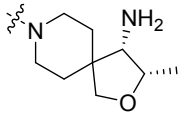	0.023	0.018	0.297	1.2/6.6	>30

Table 1. Optimization of the pyrimidinone scaffold for improved potency, hERG selectivity, and oral exposure.

In addition, **8** was membrane permeable (Caco-2 Papp A-B = 6.8 x 10^{-6} cm/s), moderately stable in rat liver microsomes (Cl_{int} = 39.3, μL/min/mg, $T_{1/2}$ = 37 min), and had no CYP inhibition (IC_{50} = > 50 μM for CYP3A4, CYP2C9 and CYP2D6). Compound **8** was next evaluated *in vivo* at 10, 30 and 100 mg/kg in mice bearing subcutaneously implanted KYSE520 xenografts. Free concentration of **8** (92 % mouse plasma protein bound) correlated well with the MAPK pathway

pharmacodynamic markers p-ERK and DUSP6. Maximal PD effects were observed at 100 mg/kg and as early as 3 hours post-dose.

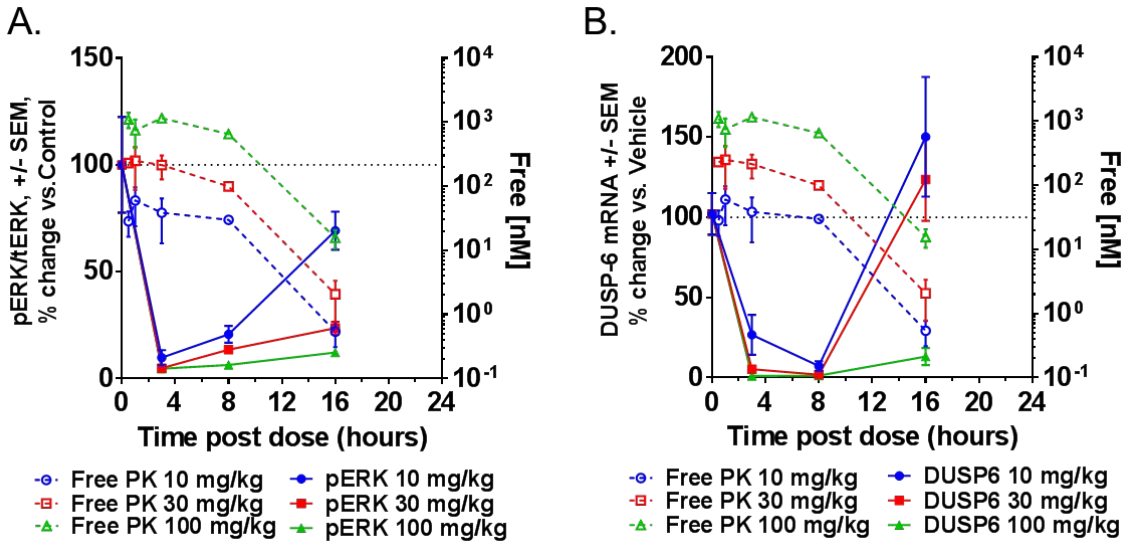

Figure 3. PK-PD of **8** in KYSE520 tumor implanted immunocompromised mice at 10, 30, and 100 mg/kg. A. p-ERK modulation in KYSE520 model. B. DUSP6 modulation in KYSE520 model.

Although robust p-ERK modulation was observed in vivo, significant hERG inhibition (**6**, **8**: IC_{50} = 4.0-6.0 μM) still plagued the series despite varying the amine pKa, presumably due to the lipophilic arene present. Redesign of the aryl group to include a pyridyl N in proximity to K492, while satisfying the hydrophobic demands of the pocket formed by L254, Q257 and P491, resulted in the more polar 2-methyl-3-chloropyridyl analog, **9**. Compound **9** retained cellular potency (antiproliferative IC_{50} = 0.220 μM), had excellent aqueous solubility (0.88 mM in pH 6.8 buffer), and no accompanying hERG inhibition (IC_{50} >30 μM). Gratifyingly, pharmacokinetic analysis in rats showed an improvement in rodent oral exposure (dose-normalized to 1 mg/kg PO, 2.01 μM·h) and bioavailability (56 %*F*) compared to **8** and 10 other tested pyrimidinones. Attempts to further improve **9** by introducing additional lipophilic functional groups in the aryl region generally resulted in no potency improvement, but increased hERG inhibition, as

exemplified by **10**. Further evolution of the aryl motif included transposition of the pyridyl nitrogen *meta* to the thioether, and introduction of an *ortho*-trifluoromethyl group resulting in **1**. Compound **1** was approximately equipotent to **9** and **10** in biochemical and cellular assays, selective over the hERG ion channel, and displayed high lipophilic efficiency (6.6).

Though the unique nature of each of these heterocycles sometimes required various synthetic approaches, many of the analogues were prepared following the synthetic route outlined for **1** (Scheme 1). Beginning with the corresponding pyrimidine-dione (**11**), the spirocyclic amine **12**[17,22] was coupled using BOP;[23] other well-precedented methods, including the synthesis of the corresponding 2-chloro-4-pyrimidones with $POCl_3$ and more modern coupling reagents, failed to provide for a number of modified core analogs in acceptable yields. The coupled product was then reacted with di-*tert*-butyl dicarbonate to afford the corresponding Boc-protected amine (**13**), which substantially improved the handling of these otherwise water soluble compounds. Selective iodination at the 2-position of the pyrimidinone ring afforded 5-iodopyrimidinone **14**, which was converted to the corresponding biaryl thioether through a copper-catalyzed Ullman reaction with **15**. A final Boc deprotection with TFA followed by HPLC purification afforded the desired product (**1**) in approximately 10% overall yield. This synthetic route was amenable to scale-up and was successfully utilized to produce **1** on multi-gram scale.

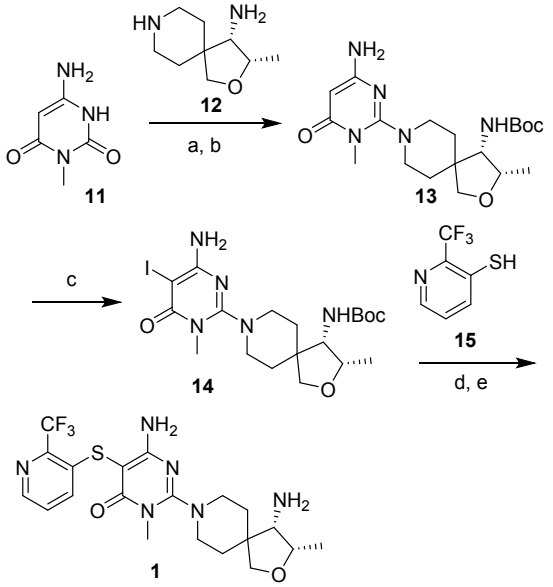

Scheme 1. Synthesis of *N*-methylamino pyrimidinone **1**. (a) Amine, BOP, DBU, DMF, RT, 3 days, 59% yield (b) Boc_2O, DIPEA, DMF, RT, 1 h, (c) NIS, DMF, RT, 10 min, 39% yield (2 steps) (d) ArSH, CuI, TMEDA, K_3PO_4, 1,4-dioxane, 100 °C, 1.5 h, (e) TFA, DCM, 3 h, 51% yield (2 steps).

Due to the encouraging initial results with peripheral fragment optimization, and the promising designs enabled by our crystal structures, we sought to further explore the minimum pharmacophore requirements around the central pyrimidinone ring. Our central ring studies began by maintaining the spiro[4.5]-amine and trifluoromethyl-pyridine in order to maintain potency and minimize hERG activity (Table 2). Removal of the 6-position NH_2 resulted in a loss in potency (**16**: p-ERK IC_{50} = 0.096 μM), and removal of the 3-Me further eroded cellular potency (**17**: p-ERK IC_{50} > 1 μM) which was reminiscent of **7**. Removal of nitrogen at the 1-position of the *N*-methylpyrimidinone resulted in pyridone **18** and aminopyridone **19**, which substantially decreased the biochemical activity. The 1-position N likely affects the R111 H-bond interaction via inductive effects on the 4-position carbonyl, and also allows for piperidine conformations preferred for binding. Taken together, the 6-amino, 3-methyl pyrimidinone, present in **1**, was optimal.

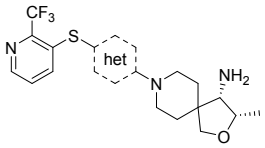

compound	core	*SHP2* IC_{50} (μM)	*p-ERK* IC_{50} (μM)	*antiproliferation* IC_{50} (μM)	*cLogP/LipE*	*hERG* IC_{50} (μM)
1	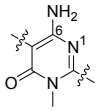	0.023	0.018	0.297	1.2/6.6	>30
16		0.026	0.096	1.5	1.5/5.9	>30
17		0.031	1.06	N.D.	1.3/6.2	>30
18		0.177	N.D.	N.D.	2.1/4.7	ND
19	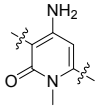	0.429	N.D.	N.D.	1.1/5.3	ND

Table 2. Systematic removal of functional groups from the core to define the minimum pharmacophore.

Our efforts to further optimize **1** via the spirocyclic amine region similarly began with efforts to improve permeability and potency by matching lipophilic fragments to the polar pyrimidinone core. Holding the trifluoromethyl-pyridine fragment constant, we prepared **20**, which bears a γ-methylamino spiro[4.5]-amine lacking the cyclic ether common to **1** and **8-10**. This compound showed similar gains in cellular potency to those observed for **8** while crucially maintaining selectivity against hERG (IC_{50} >30 μM). Disappointingly, rat pharmacokinetic data indicated that this compound had very poor oral exposure (6 mg/kg PO, 0.03 μM·h) and bioavailability (1 %*F*). *In vitro* microsomal clearance (Cl_{int} = 3.4 μL/min/mg, $T_{1/2}$ = 6.6 h in rat liver microsomes) and permeability (Caco-2 Papp A-B < 0.5 x 10^{-6} cm/s) data suggested these inadequate pharmacokinetic properties resulted from poor permeability and absorption, which we attributed to the more basic and less sterically encumbered primary amine in **20**. In order to

improve the properties of **20**, we introduced a fluorine β to the amine (e.g., **21**), thus reducing the pKa of the amine via an inductive effect.[24] Although **21** showed promising potency (less than two-fold reduction in antiproliferation potency compared to **20**), the synthetic challenge of a molecule bearing three contiguous stereocenters adjacent to a spirocyclic center on a cyclopentyl ring reduced the attractiveness of this analogue when compared to other analogs (e.g., **1**, **9**). The increased lipophilicity of **21** (cLogP = 2.3) compared to **1** and **9** (cLogP = 1.2, 1.5, respectively) further reduced the desire to pursue this synthetically challenging target.

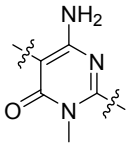

compound	Ar-	amine	*SHP2* IC_{50} (μM)	*p-ERK* IC_{50} (μM)	*antiproliferation* IC_{50} (μM)	*cLogP/LipE*	*hERG* IC_{50} (μM)
1	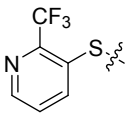	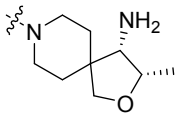	0.023	0.018	0.297	1.2/6.6	>30
20	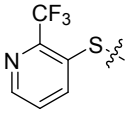	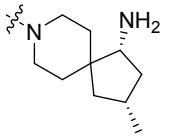	0.022	0.004	0.098	2.3/6.2	>30
21	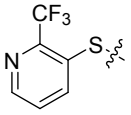	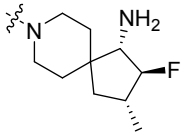	0.018	0.005	0.160	2.1/5.9	>30

Table 3. Select spirocyclic amine SAR

Given the acceptable *in vitro* potency and hERG selectivity of pyrimidinone **1**, we next investigated its selectivity, physicochemical and pharmacokinetic properties. Initial evaluation against a standard kinase and safety pharmacology panel (consisting of ion channels, kinases, GPCRs) showed no evidence of off-target activity, suggesting that the pyrimidinone series possessed the same overall selectivity observed for the aminopyrazines. The overall polarity of **1** enabled excellent aqueous solubility (0.98 mM in pH 6.8 buffer), but low permeability (Papp(A-

B) 1.02 x 10^{-6} cm/s), and apparent efflux (B-A/A-B = 15) in Caco-2 cells. The metabolic stability of **1** in both rat and mouse liver microsomes indicated low clearance (Cl_{int} = 7.9-11.1 μL/min/mg; $T_{1/2}$ > 2 h) for both species. Subsequent pharmacokinetic studies of **1** in rat confirmed low clearance (Cl_{int} = 21 μL/min/mg; $T_{1/2}$ = 10.9 h), moderate oral exposure (dose-normalized to 1 mg/kg PO, 0.45 μM·h) and oral bioavailability (29 %*F*). We speculate that low membrane permeability and efflux contributed to this moderate oral exposure.

With the acceptable disposition of **1** in rat, and the previous demonstration of p-ERK and DUSP6 modulation in the KYSE520 model by **8**, we next sought to broaden our characterization of the series across cancer cell lineages. We evaluated **1** in the Detroit-562 pharyngeal carcinoma cell line *in vitro* (antiproliferative IC_{50} = 1.38 μM), and compared it to other inhibitors (**8**: IC_{50} = 0.35 μM; **2** (SHP099): IC_{50} = 6.47 μM; SHP389[17]: IC_{50} = 4.13 μM). Although the absolute IC_{50} was perturbed as compared to the KYSE520 cells, possibly due to the differences in cell lines and p-ERK assays, the rank order of compound potency across the two models remained constant. We also evaluated **1** in the Detroit-562 mouse model, with tumors subcutaneously implanted into immunocompromised mice (Figure 4). Single rising doses of 20, 40, and 80 mg/kg dosed twice daily, led to dose-dependent exposure and reduction in expression of pharmacodynamic marker DUSP6 mRNA (Figure 4A). An efficacy study employing 20, 40, and 80 mg/kg BID dosing of **1** demonstrated a clear dose-dependent reduction in tumor volume. Approximate tumor stasis was observed by 21 days at the well-tolerated dose of 40 mg/kg twice daily (11% T/C), and tumor regression was achieved at 80 mg/kg twice daily (34 % regression) after dosing for 14 days, with a mean reduction on mouse host bodyweight (-2.2 % from first dose).

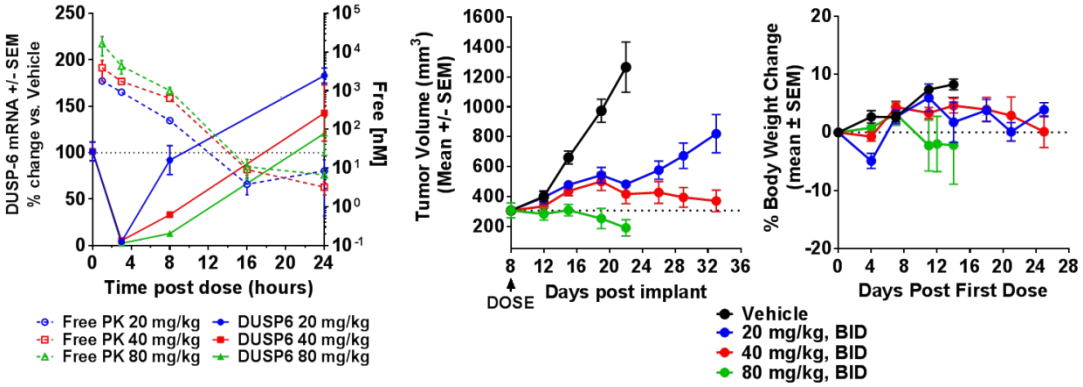

Figure 4. PK/PD and efficacy of **1** in pharyngeal carcinoma Detroit-562 xenograft model.

DISCUSSION AND CONCLUSIONS

The development of potent, selective, and orally efficacious SHP2 inhibitors presents an important challenge due to the increasingly appreciated biological significance of this oncogenic protein tyrosine phosphatase in cancer, stromal, and immune cells. Following our discovery of an allosteric pocket that enables stabilization of an autoinhibited conformation, we have pursued several classes of SHP2 inhibitors and clinical investigation is underway.[25] In this manuscript, we apply SAR across aminopyrazine (e.g., **2**), 5,6-fused bicyclic (e.g., **3**), and 6,5-fused bicyclic (e.g., **5**) chemical templates in conjunction with X-ray crystallographic data to originate a monocyclic pyrimidinone scaffold with high lipophilic efficiency. The minimum pharmacophore requirements of the central scaffold were determined, and the potency and ADME properties of the pyrimidinones were further improved. These studies culminated in the identification of **1**, which showed correlative and dose-dependent PK, PD and efficacy when dosed orally to immunocompromised mice bearing subcutaneously implanted Detroit-562 tumor cells. Further perturbation of the aryl thioether and spiro[4.5]-amine moieties resulted in the synthesis of a number of related analogues with similar antiproliferation potency to **1**. Notably, **8** improved upon the potency, and **9** improved the oral exposure and hERG selectivity as compared to **1**. Aminopyrimidinones **1**, **8**, **9**, and the additional analogues described here provide compelling

potent, selective, and orally bioavailable alternatives to previously disclosed SHP2 inhibitors for future investigation of the multifaceted roles of SHP2 in signal transduction and human disease.

EXPERIMENTAL SECTION

Compound synthesis and characterization. Compound purity was assessed by HPLC to confirm > 95% purity. All solvents employed were commercially available anhydrous grade, and reagents used as received unless otherwise noted. Purification of intermediates and final products was carried out on a normal phase using an ISCO CombiFlash system and prepacked SiO_2 cartridges eluted with optimized gradients of either ethyl acetate/heptane mixture or methanol/dichloromethane as described. Preparative high pressure liquid chromatography (HPLC) was performed using a Waters 2525 pump with 2487 dual wavelength detector and 2767 sample manager. Columns were Waters C18 OBD 5 μm, either 50x100 mm Xbridge or 30x100 mm Sunfire. NMR spectra were recorded on a Bruker AV400 (Avance 400 MHz) or AV600 (Avance 600 MHz) instruments. Analytical LC-MS was conducted using an Agilent 1100 series with UV detection at 214 nm and 254 nm, and an electrospray mode (ESI) coupled with a Waters ZQ single quad mass detector. One of two methods was used: Method A) 5-95% acetonitrile/H_2O with 5 mM ammonium formate with a 2 min run, 3 μL injection through an inertisil C8 3 cm x 5 mm x 3μm; Method B) 20-95% acetonitrile/H_2O with 10 mM ammonium formate with a 2 min run, 3 μL injection through an inertisil C8 3 cm x 5 mm x 3 μm. Purity of all tested compounds was determined by LC/ESI-MS, data recorded using an Agilent 6220 mass spectrometer with electrospray ionization source and Agilent 1200 liquid chromatography. The mass accuracy of the system has been found to be < 5 ppm. HPLC separation was performed at 75 mL/min flow rate

with the indicated gradient within 3.5 min with an initial hold of 10 seconds. 10 mM ammonia hydroxide or 0.1 M TFA was used as the modifier additive in the aqueous phase.

Preparation of 6-Amino-2-((3S,4S)-4-amino-3-methyl-2-oxa-8-azaspiro[4.5]decan-8-yl)-3-methyl-5-((2-(trifluoromethyl)pyridin-3-yl)thio)pyrimidin-4(3H)-one (1). A mixture of 6-amino-3-methylpyrimidine-2,4(1H,3H)-dione (1 g, 7.09 mmol), (3*S*,4*S*)-3-methyl-2-oxa-8-azaspiro[4.5]decan-4-amine (1.81 g, 7.44 mmol), BOP (6.27 g, 14.17 mmol), and DBU (7.48 mL, 49.6 mmol) in DMF (15 mL) was stirred for 60 h at RT. The resulting mixture was purified by HPLC (gradient elution 2-12% MeCN in water, 5 mM NH_4OH modifier) to give 6-amino-2-((3*S*,4*S*)-4-amino-3-methyl-2-oxa-8-azaspiro[4.5]decan-8-yl)-3-methylpyrimidin-4(3H)-one (2.08 g, 7.09 mmol). MS *m/z* 294.3 $(M+H)^+$.

A mixture 6-amino-2-((3*S*,4*S*)-4-amino-3-methyl-2-oxa-8-azaspiro[4.5]decan-8-yl)-3-methylpyrimidin-4(3H)-one (2.08 g, 7.09 mmol), Boc2O (1.55 g, 7.09 mmol), and DIPEA (2.5 mL, 14.18 mmol) in DMF (14 mL) was stirred for 1 h at RT. The resulting mixture was poured into a separation funnel containing sat. aq. NH_4Cl (75 mL) and it was extracted with DCM (3 x 15 mL). The combined organic phases were dried over $MgSO_4$, filtered, and the volatiles were removed under reduced pressure to give *tert*-butyl ((3*S*,4*S*)-8-(4-amino-1-methyl-6-oxo-1,6-dihydropyrimidin-2-yl)-3-methyl-2-oxa-8-azaspiro[4.5]decan-4-yl)carbamate (2.79 g, 7.09 mmol). MS *m/z* 394.4 $(M+H)^+$. This compound was used in next step without futher purification.

A mixture of *tert*-butyl ((3*S*,4*S*)-8-(4-amino-1-methyl-6-oxo-1,6-dihydropyrimidin-2-yl)-3-methyl-2-oxa-8-azaspiro[4.5]decan-4-yl)carbamate (2.79 g, 7.09 mmol) and NIS (1.76 g, 7.80 mmol) in DMF (14 mL) was stirred for 1 h at RT. The resulting mixture was poured into a separation funnel containing sat. aq. $Na_2S_2O_3$ (25 mL), sat. aq. NH_4Cl (25 mL), and water (25 mL) and was extracted with DCM (3 x 20 mL). The combined organic phases were dried over MgSO4,

filtered, the volatiles were removed under reduced pressure, and the residue was purified by silica chromatography (0 to 5% gradient of MeOH/DCM) to give *tert*-butyl ((3*S*,4*S*)-8-(4-amino-5-iodo-1-methyl-6-oxo-1,6-dihydropyrimidin-2-yl)-3-methyl-2-oxa-8-azaspiro[4.5]decan-4-yl)carbamate (1.51 g, 2.91 mmol). MS *m/z* 520.1 $(M+H)^+$.

A mixture of *tert*-butyl ((3*S*,4*S*)-8-(4-amino-5-iodo-1-methyl-6-oxo-1,6-dihydropyrimidin-2-yl)-3-methyl-2-oxa-8-azaspiro[4.5]decan-4-yl)carbamate (42 mg, 0.081 mmol), 2-(trifluoromethyl)pyridine-3-thiol (22 mg, 0.121 mmol), CuI (3.1 mg, 0.016 mmol),TMEDA (5 µL, 0.032 mmol), and K_3PO_4 (51 mg, 0.243 mmol) in dioxane (0.5 mL) was stirred for 90 min at 100 °C. After cooling to RT, the reaction mixture was poured into a separationfunnel containing aq. K_2CO_3 (2 M, 2 mL) and extracted with DCM (3 x 5 mL). The combined organic phases were dried over $MgSO_4$, filtered, and the volatiles were removed under reduced pressure. The residue was dissolved in DCM (5 mL) and TFA (1 mL) was added. After stirring for 20 min at RT, the volatiles were removed under reduced pressure and the residue was purified by HPLC (gradient elution 15-40% MeCN in water, 5 mM NH_4OH modifier) to give 6-amino-2-((3*S*,4*S*)-4-amino-3-methyl-2-oxa-8-azaspiro[4.5]decan-8-yl)-3-methyl-5-((2-(trifluoromethyl)pyridin-3-yl)thio)pyrimidin-4(3H)-one (**1**) as a white solid (20.0 mg, 0.043 mmol). ^{1}H NMR (400 MHz, methanol-d_4) δ ppm 8.24-8.41 (m, 1 H), 7.51 (d, J=7.58 Hz, 1 H), 7.41 (dd, J=8.34, 4.55 Hz, 1 H), 4.22 (dd, J=6.32, 5.05 Hz, 1 H), 3.84 (d, J=8.84 Hz, 1 H), 3.69 (d, J=8.59 Hz, 1 H), 3.47-3.61 (m, 2 H), 3.36-3.47 (m, 3 H), 3.04-3.26 (m, 2 H), 3.03 (d, J=5.05 Hz, 1 H), 1.79-2.02 (m, 2 H), 1.60-1.78 (m, 2 H), 1.13-1.28 (m, 3 H). ^{19}F NMR (376 MHz, methanol-d_4) δ ppm -66.36. HRMS calcd for $C_{20}H_{26}F_3N_6O_2S$ $(M+H)^+$ 471.1790, found 471.1809.

Protein Expression and Purification. The gene encoding human SHP2 from residues Met1−Leu525 was inserted into a pET30 vector. A coding sequence for a 6× histidine tag followed by a TEV protease consensus sequence was added 5′ to the SHP2 gene sequence. The construct was transformed into BL21 Star (DE3) cells and grown at 37 °C in Terrific Broth containing 100 μg/mL kanamycin. At an OD600 of 4.0, SHP2 expression was induced using 1 mM IPTG. Cells were harvested following overnight growth at 18 °C.

Cell pellets were resuspended in lysis buffer containing 50 mM Tris-HCl, pH 8.5, 25 mM imidazole, 500 mM NaCl, 2.5 mM MgCl2, 1 mM TCEP, 1 μg/mL DNase1, and complete EDTA-free protease inhibitor and lysed using a microfluidizer, followed by ultracentrifugation. The supernatant was loaded onto a HisTrap HP chelating column in 50 mM Tris-HCl, 25 mM imidazole, 500 mM NaCl, 1 mM TCEP and protein was eluted with the addition of 250 mM imidazole. The Nterminal histidine tag was removed with an overnight incubation using TEV protease at 4 °C. The protein was subsequently diluted to 50 mM NaCl with 20 mM Tris-HCl, pH 8.5, 1 mM TCEP, then applied to a HiTrap Q FastFlow column equilibrated with 20 mM Tris, pH 8.5, 50 mM NaCl, 1 mM TCEP. The protein was eluted with a 10 column volume gradient from 50 to 500 mM NaCl. Fractions containing SHP2 were pooled and concentrated then loaded onto a HiLoad Superdex200 PG 16/100 column, exchanging the protein into the crystallization buffer, 20 mM Tris-HCl, pH 8.5, 150 mM NaCl, and 3 mM TCEP. The protein was concentrated to 15 mg/mL for use in crystallization. Crystallization, DSF, and high throughput screening assays used the 1−525 construct of SHP2, while biochemical assays used the 2−593 construct.

Biochemical Assay. SHP2 is allosterically activated through binding of bis-tyrosyl-phorphorylated peptides to its Src Homology 2 (SH2) domains. The latter activation step leads to the release of the autoinhibitory interface of SHP2, which in turn renders the SHP2 PTP active and

available for substrate recognition and reaction catalysis. The catalytic activity of SHP2 was monitored using the surrogate substrate DiFMUP in a prompt fluorescence assay format. More specifically, the phosphatase reactions were performed at room temperature in 384-well black polystyrene plate, flat bottom, low flange, nonbinding surface (Corning, cat. no. 3575) using a final reaction volume of 25 μL and the following assay buffer conditions: 60 mM HEPES, pH 7.2, 75 mM NaCl, 75 mM KCl, 1 mM EDTA, 0.05 % P-20, 5 mM DTT.

The inhibition of SHP2 from the tested compounds (concentrations varying from 0.003 to 100 μM) was monitored using an assay in which 0.5 nM of SHP2 was incubated with of 0.5 μM of peptide IRS1_pY1172(dPEG8)pY1222(sequence H2N-LN(pY)IDLDLV-(dPEG8)LST(pY)ASINFQK-amide). After 30−60 min incubation at 25 °C, the surrogate substrate DiFMUP (Invitrogen, cat. no. D6567, 200 μM) was added to the reaction and incubated at 25 °C for 30 min (200 μM for residue 2−593, 100 μM for residue 1−525 construct). The reaction was then quenched by the addition of 5 μL of a 160 μM solution of bpV(Phen) (Enzo Life Sciences cat. no. ALX-270−204). The fluorescence signal was monitored using a microplate reader (Envision, Perki-Elmer) using excitation and emission wavelengths of 340 and 450 nm, respectively. The inhibitor dose−response curves were analyzed using normalized IC50 regression curve fitting with control based normalization.

Cellular Assay. p-ERK cellular assay using the AlphaScreen SureFire Phospho-ERK 1/2 Kit (PerkinElmer) was performed as follows: KYSE520 cells (30,000 cells/well) were grown in 96-well plate culture overnight and treated with SHP2 inhibitors at concentrations of 20, 6.6, 2.2, 0.74, 0.24, 0.08, and 0.027 μM for 2 h at 37 °C. Incubations were terminated by addition of 30 μL of lysis buffer (PerkinElmer) supplied with the SureFire phospho-extracellular signal-regulated kinase (p-ERK) assay kit (PerkinElmer). Samples were processed according to the manufacturer's

directions. The fluorescence signal from p-ERK was measured in duplicate using a 2101 multilabel reader (PerkinElmer Envision). The percentage of inhibition was normalized by the total ERK signal and compared with the DMSO vehicle control.

Cell Proliferation Assay. Cells (1500-cells/well) were plated onto 96-well plates in 100 μL medium (RPMI-1640 containing 10% FBS, Lonza). Compounds with various concentrations (1.25, 2.5, 5, 10, and 20 μM) were added 24 h after cell plating. At day 5, 50 μL of Celltiter-Glo reagent (Promega) was added, and the luminescent signal was determined according to the supplier's instruction (Promega).

Crystallization and Structure Determination. Sitting drop vapor diffusion method was used for crystallization, with the crystallization well containing 17% PEG 3350 and 200 mM ammonium phosphate and a drop with a 1:1 volume of SHP2 protein and crystallization solution. Crystals were formed within 5 days and subsequently soaked in the crystallization solution with 2.5 mM of 2. This was followed by cryoprotection using the crystallization solution with the addition of 20% glycerol and 1 mM compound **7**, followed by flash freezing directly into liquid nitrogen.

Diffraction data for the SHP2/compound **2** and SHP2/compound **3** complexes are reported elsewhere,[12,17] and those for SHP2/compound **7** complex (PDB accession *6MD7)* were collected on a Dectris Pilatus 6M detector at beamline 17ID (IMCA-CAT) at the Advanced Photon Source at Argonne National Laboratories. The data were measured from a single crystal maintained at 100 K at a wavelength of 1 Å, and the reflections were indexed, integrated, and scaled using XDS.[26] The spacegroup of the complex was P21 with two molecules in the asymmetric unit. The structure was determined with Fourier methods, using the SHP2 apo structure[13] (PDB accession *2SHP*) with all waters removed. Structure determination was achieved through iterative rounds of positional and simulated annealing refinement using BUSTER,[27] with model building using

COOT.[28] Individual B-factors were refined using an overall anisotropic B-factor refinement along with bulk solvent correction. The solvent, phosphate ions, and inhibitor were built into the density in later rounds of the refinement. Data collection and refinement statistics are shown in Table 1 of the Supporting Information.

Pharmacokinetics. All animal related procedures were conducted under a Novartis IACUC approved protocol in compliance with Animal Welfare Act regulations and the Guide for the Care and Use of Laboratory Animals. Male C57BL/6 mice were obtained from Harlan Laboratories. Following iv administration (via tail vein) at 1 mg/kg, approximately 50 μL of whole blood was collected via tail transection, at 0.083, 0.5, 1, 2, 4, and 7 h postdose and transferred to an Eppendorf microcentrifuge tube containing EDTA. Oral administration (at 5 mg/kg) and collection procedures were similar to IV, except with whole blood collection at 0.25, 0.5, 1, 2, 4, and 7 h. The blood was centrifuged at 5000 rpm, and plasma was transferred to a Matrix 96 well plate, capped, and stored frozen (−20 °C) for parent compound analysis. Samples were precipitated and diluted with acetonitrile containing internal standard and prepared for LC/MS/MS. An aliquot (20 μL) of each sample was injected into an API4000 LC/MS/MS system for analysis, and transitions of 352.05 amu (Q1) and 267.10 amu (Q3) were monitored. All pharmacokinetic (PK) parameters were derived from concentration−time data by noncompartmental analyses. All PK parameters were calculated with the computer program WinNonlin (Version 6.4) purchased from Certara Company (St. Louis, MO). For the intravenous dose, the concentration of unchanged compound at time 0 was calculated based on a log−linear regression of first two data points to back-extrapolate C(0). The area under the concentration−time curve (AUClast) was calculated using the linear trapezoidal rule.

The bioavailability was estimated as the following equation:

$$\%F = \frac{AUC_{\text{inf},p.o.}}{AUC_{\text{inf},i.v.}} \cdot \frac{Dose_{i.v.}}{Dose_{p.o.}}$$

Results are expressed as mean. No further statistical analysis was performed.

Tumor Xenograft Experiments. All animal studies were carried out according to the Novartis Guide for the Care and Use of Laboratory Animals. Six-week old female athymic NU/NU mice (Charles River Labs, MA), were inoculated subcutaneously with either KYSE520 esophageal carcinoma cells (ATCC) at a concentration of 2 x 10^6, or Detroit-562 pharyngeal carcinoma cells (ATTC) at a concentration of 5 x 10^5 , in a suspension containing 50% phenol red-free matrigel (BD Biosciences) in Hank's balanced salt solution. For all PK/PD studies, mice were administered a single dose of vehicle control (0.5% Methylcellulose, 0.1% Tween 80), **1** or **8**, by oral gavage once tumors reached roughly 300 mm^3. Mice were subsequently euthanized at predetermined time points following a single dose of compound at which point plasma and xenograft fragments were harvested for determination of 1 or 8 plasma concentrations and PD modulation. Phospho-ERK PD assessment was carried on lysed frozen tumor tissue fragments following the protocol provided by the Mesoscale Discovery assay whole cell lysis kits (Catalog#: Total ERK1/2: K151DXD, phospho-ERK1/2: K151DWD). Protein concentration was assessed by BCA (Pierce, Catalog # 23225) and 2.5mg, for total-ERK, or 20 mg for phospho-ERK, were loaded onto mesoscale plates. Samples were analyzed by a Mesoscale plate reader. Data was analyzed and fold change in phospho-ERK1/2 levels were calculated by normalizing to total ERK concentrations and the ratio of phospho-ERK/total-ERK in the vehicle treated group. DUSP6 PD assessment was carried out by quantitative real-time PCR. Frozen tumor fragments were processed to extract mRNA (Qiagen #74106). RNA quantification was performed using Nanodrop 8000. One-step qPCR (Qiagen, #204645) was performed on the 7900 HT Fast Real-Time PCR system (Themo Fisher Scientific)

using a human DUSP6 primer set (Hs00737962, Life Technologies) multiplexed with a housekeeping gene control primer, HPO (#4326314E, Life Technologies). Data was analyzed and normalized to the expression of a housekeeping gene, human ribosomal protein lateral stalk subunit P0, HPO, in order to calculate the fold change in mRNA expression with and without compound treatment. For in vivo efficacy studies, subcutaneously implanted Detroit-562 tumor xenografts were measured in the two dimensions length and width (l and w, respectively) with digital calipers once to twice weekly from the start of dosing. Tumor volume was calculated using a modified ellipsoid formula, where tumor volume (TV) (mm^3) = [((l x w2) x 3.14159)) / 6], where l is the longest axis of the tumor and w is perpendicular to l. Detroit-562 tumor bearing mice were randomized into treatment groups based on tumor volume mean of 300 mm^3 and were dosed by oral gavage twice daily.

ANCILLARY INFORMATION

Supporting information. The Supporting Information is available free of charge on the ACS Publications website (insert DOI here), which includes X-ray data table, additional synthetic procedures, and Molecular Formula Strings.

Accession Codes. *6MD7* for SHP2 in complex with compound **7**. Authors will release the atomic coordinates and experimental data upon article publication.

Corresponding author. Email: matthew.lamarche@novartis.com; telephone: 617-871-7729. Novartis Institutes for Biomedical Research, Inc. 250 Massachusetts Avenue, Cambridge, MA 02139.

Author Contributions. The manuscript was written through contributions of all authors.

All authors have given approval to the final version of the manuscript.

Notes. The authors declare no competing financial interest.

Acknowledgements. Use of the IMCA-CAT beamline 17-ID at the Advanced Photon Source was supported by the companies of the Industrial Macromolecular Crystallography Association through a contract with Hauptman-Woodward Medical Research Institute. Use of the Advanced Photon Source was supported by the U.S. Department of Energy, Office of Science, Office of Basic Energy Sciences, under Contract No. DE-AC02-06CH11357. The authors thank Yue Pan, Dan Palacios, Joe Wzorek, Jonathan Hempel for editing suggestions, and the entire SHP2 team.

Abbreviations used. PTP, protein tyrosine phosphatase; RAS, rat sarcoma protein; AKT, protein kinase B; JAK, Janus kinase; STAT, Signal Transducer and Activator of Transcription proteins. ERK, extracellular signal-regulated kinase; PI3K, phosphoinositide 3-kinase; MAPK, mitogen-activated protein kinase; TCEP, tris(2-carboxyethyl)phosphine; IPTG, isopropyl β-D-1-thiogalactopyranoside; EDTA, ethylenediaminetetraacetic acid; HEPES, 4-(2-hydroxyethyl)-1-piperazineethanesulfonic acid; DTT, dithiothreitol.

REFERENCES.

1. Tartaglia, M.; Mehler, E. L.; Godberg, R.; Zampino, G.; Brunner H. G.; Kremer, H.; Van Der Burgt, I.; Crosby, A. H.; Ion, A.; Jeffery, S.; Kalidas, K.; Patton, J. A.; Kucherlapati, R. S.; Gelb, B. D. Mutations in *Ptpn11*, Encoding the Protein Tyrosine Phosphatase SHP-2, Cause Noonan syndrome. *Nat. Genet.* **2001**, *29*, 465-468.

2. (a) Tartaglia, M.; Niemeyer, C. M.; Fragale, A.; Song, X.; Buechner, J.; Jung, A.; Hählen, K.; Hasle, H.; Licht, J. D.; Gelb, B. D. Somatic Mutations in *Ptpn11* in Juvenile Myelomonocytic Leukemia, Myelodysplactic Syndromes and Acute Myeloid Leukemia. *Nat. Genet.* **2003**, *34*, 148-150. (b) Mulero-Navarro, S.; Sevilla, A.; Roman, A. C.; Lee, D.-F.; D'Souza, S. L.; Pardo, S.;

Riess, I.; Su, J.; Cohen, N.; Schaniel, C.; Rodriguez, N. A.; Baccarini, A.; Brown, B. D.; Cavé, A.; Strullu, M.; Yalcin, S.; Park, C. Y.; Dhandapany, P.S.; Yongchao, G.; Edelmann, L.; Bahieg, S.; Raynal, P.; Flex, E.; Tartaglia, M.; Moore, K. A.; Lemishka, I. R.; Gelb, B. D. Myleoid Dysregulation in a Human Induced Pluripotent Stem Cell Model of *Ptpn11*-Associated Juvenile Myleomonocytic Leukemia. *Cell Rep.* **2015,** *13,* 504-515.

3. (a) Bentires-Alj, M.; Paez, J. G.; David, F. S.; Keilhack, H.; Halmos, B.; Naoki, K.; Maris, J. M.; Richardson, A.; Bardelli, A.; Sugarbaker, D. J.; Richards, W. G.; Du, J.; Girard, L.; Minna, J. D.; Loh, M. L.; Fisher, D. E.; Velculescu, V. E.; Vogelstein, B.; Meyerson, M.; Sellers, W. R.; Neel, B. G. Activating Mutations of the Noonan Syndrome-Associated SHP2/*Ptpn11* Gene in Human Solid Tumors and Adult Acute MyelogenousLeukemia. *Cancer Res.* **2004,** *64,* 8816−8820. (b) Chan, G.; Kalaitzidis, D.; Neel, B. G. The Tyrosine Phosphoatase Shp2 (*Ptpn11*) in Cancer. *Cancer Metastasis Rev.* **2008,** *27,* 179-192. (c) Miyamoto, D.; Miyamoto, M.; Takahashi, A.; Yomogita, Y.; Hagashi, H.; Kondo, S.; Hatakeyama, M. Isolation of a Distinct Class of Gain-of-Function SHP-2 mutants with Oncogenic RAS-like Transforming Activity From Solid Tumors. *Oncogene* **2008,** *27,* 3508-3515.

4. (a) Neel, B. G.; Gu, H.; Pao, L. The 'Shp'ing News: SH2 Domain-Containing Tyrosine Phosphatases in Cell Signaling. Trends *Biochem. Sci.* **2003,** *28,* 284-293. (b) Chan, R. J.; Feng, G. S. *Ptpn11* is the First Identified Proto-Oncogene That Encodes a Tyrosine Phosphatase. *Blood* **2007,** *109,* 862-867. (c) Tiganis, T.; Bennett, A. M. Protein Tyrosine Phosphatase Function: the Substrated Perspective. *Biochem. J.* **2007,** *402,* 1-15.

5. Li, J.; Jie, H.-B.; Lei, Y.; Gildener-Leapman, N.; Trivedi, S. PD-1/SHP-2 Inhibits Tc1/Th1 Phenotypic Responses and the Activation of T Cells in the Tumor Microenvironment. *Cancer Res.* **2015**, *75*, 508-518.

6. Hui, E.; Cheung, J.; Zhu, J.; Su, X. ; Taylor, M.J. ; Wallweber, H.A. ; Sasmal, D.K.; Huang, J.; Kim, J.M.; Mellman, I.; Vale, R.D. T Cell Costimulatory Receptor CD28 is a Primary Target for PD-1-Mediated Inhibition. *Science*, **2017**, 355, 1428-1433. DOI: 10.1126/science.aafl292

7. Butterworth, S.; Overduin, M.; Barr, A. J.; Targeting Protein Tyrosine Phosphatase SHP2 for Therapeutic Intervention. *Future Med. Chem.,* **2014** , *6*, 1423-1437.

8. (a) Chen, L.; Sung, S.-S.; Yip, M. L. R.; Lawrence, H. R.; Ren, Y.; Guida, W. C.; Sebti, S. M.; Lawrence, N. J.; Wu, J. Discovery of a Novel Shp2 Protein Tyrosine Phosphatase Inhibitor. *Mol. Pharmacol.* **2006,** *70,* 562-570. (b) Chen, C.; Cao, M.; Zhu, S.; Wang, C.; Liang, F.; Yan, L.; Luo, D. Discovery of a Novel Inhibitor of the Protein Tyrosine Phosphatase Shp2. *Scientific Reports* **2015,** *5,* 17626. c) Chen, C.; Liang, F.; Chen, B.; Sun, Z.; Xue, T.; Yangm R.; Luo, D. Identification of demethylincisterol A_3 as a Selective Inhibitor of Protein Tyrosine Phosphatase Shp2. *Eur. J. Pharmacol.* **2017,** *795,* 124-133. (d) Grosskopf, S.; Eckert, C.; Arkona, C.; Radetzki, S.; Böhm, K.; Heinemann, U.; Wolber, G.; von Kries, J.P.; Birchmeier, W.; Rademann, J. Selective Inhibitors of the Protein Tyrosine Phosphatase SHP2 Block Cellular Motility and Growth of Cancer Cells In Vitro and In Vivo. *ChemMedChem.* **2015,** 5, 815-826. doi: 10.1002/cmdc.201500015.

9. (a) Bialy, L.; Waldmann, H. Inhibitors of Protein Tyrosine Phosphatases: Next Generation Drugs? *Angew. Chem. Int. Ed.* **2005,** *44,* 3813-3839. (b) Scott, L. M.; Lawrence, H. R.; Sebti, S. M.; Lawrence, N. J.; Wu, J. Targeting Protein Tyrosine Phosphatases for Anticancer Drug Discovery. *Curr. Pharm. Des.* **2010,** *16,* 1843−1862.

10. (a) Gilmartin, A.G.; Faitg, T.H.; Richter, M.; Groy, A.; Seefeld, M.A.; Darcy, M.G.; Peng, X.; Federowicz, K.; Yang, J.; Zhang, S.Y.; Minthorn, E.; Jaworski, J.P.; Schaber, M.; Martens, S.; McNulty, D.E.; Sinnamon, R. H.; Zhang, H.; Kirkpatrick, R.B.; Nevins, N.; Cui, G.; Pietrak, B.;

Diaz, E.; Jones, A.; Brandt, M.; Schwartz, B.; Heerding, D.A.; Kumar, R. Allosteric WIP1 Phosphatase Inhibition Through Flap-Subdomain Interaction. *Nat. Chem. Biol.* **2014,** *10,* 181-187. (b) Chio, C. M.;Yu, X.; Bishop, A. C. Rational Design of Allosteric-Inhibition Sites in Classical Protein Tyrosine Phosphatases. *Bioorg. Med. Chem.* **2015,** *23,* 2828-2838. (c) Schneider, R.; Beumer, C.; Simard, J. R.; Grutter, C.; Rauh, D. Selective Detection of Allosteric Phosphatase Inhibitors. *J. Am. Chem. Soc.* **2013,** *135,* 6838-6841.

11. Chen, Y.P.; LaMarche, M.J.; Fekkes, P.; Garcia–Fortanet, J.; Acker, M.; Chan, H.; Chen, Z.; Deng, Z.; Fei, F.; Firestone, B.; Fodor, M.; Gao, H.; Ho, S.; Hsiao, K.; Kang, Z.; Keen, .N; Labonte, L.; Liu, S.; Meyer, M.; Pu, M.; Price, E.; Ramsey, T.; Slisz, J.; Wang, P.; Yang, G.; Zhang, J.; Zhu, P.; Sellers, W.R.; Stams, T.; Fortin, P.D. Discovery of an Allosteric SHP2 Inhibitor for Cancer Therapy. *Nature*, **2016**, *535*, 148–152.

12. Fortanet, J. G.; Chen, C. H.-T.; Chen, Y.-N. P.; Chen, Z.; Deng, Z.; Firestone, B.; Fekkes, P.; Fodor, M.; Fortin, P. D.; Fridrich, C.; Grunenfelder, D.; Ho, S.; Kang, Z. B.; Karki, R.; Kato, M.; Keen, N.; LaBonte, L. R.; Larrow, J.; Lenoir, F.; Liu, G.; Liu, S.; Lombardo, F.; Majumdar, D.; Meyer, M. J.; Palermo, M.; Perez, L.; Pu, M.; Ramsey, T.; Sellers, W. R.; Shultz, M. D.; Stams, T.; Towler, C.; Wang, P.; Williams, S. L.; Zhang, J.-H.; LaMarche, M. J. Allosteric Inhibition of SHP2: Identification of a Potent, Selective, and Orally Efficacious Phosphatase Inhibitor. *J. Med. Chem.* **2016,** *59*, 7773-7782.

13. (a) Hof, P.; Pluskey, S.; Dhe-Paganon, S.; Eck, M. J.; Shoelson, S. E. Crystal Structure of the Tyrosine Phosphatase SHP-2. *Cell* **1998,** *92,* 441−450. (b) Barford, D.; Neel, B. G. Revealing Mechanisms for SH2 Domain Mediated Regulation of the Protein Tyrosine Phosphatase SHP-2. *Structure* **1998,** *6,* 249−254.

14. (a) LaRochelle, J.R.; Fodor, M.; Xu, X.; Durzynska, I.; Fan, L.; Stams, T.; Chan, H.M.; LaMarche, M.J.; Chopra, R.; Wang, P.; Fortin, P.D.; Acker, M.G.; Blacklow, S.C.; Structural and Functional Consequences of Three Cancer-Associated Mutations of the Oncogenic Phosphatase SHP2. *Biochemistry.* **2016,** 55, 2269-2277. doi: 10.1021/acs.biochem.5b01287. (b) LaRochelle, J.R.; Fodor, M.; Ellegast, J.M.; Liu, X.; Vemulapalli, V.; Mohseni, M.; Stams, T.; Buhrlage, S.J.; Stegmaier, K.; LaMarche, M.J.; Acker, M.G.; Blacklow, S.C. Identification of an Allosteric Benzothiazolopyrimidone Inhibitor of the Oncogenic Protein Tyrosine Phosphatase SHP2. *Bioorg Med Chem*., **2017**, 25, 6479-6485. doi: 10.1016/j.bmc.2017.10.025.

15. Xie, J.; Si, X.; Gu, S.; Wang, M.; Shen, J.; Li, H.; Shen, J.; Li, D.; Fang, Y.; Liu, C.; Zhu, J.; Allosteric Inhibitors of SHP2 with Therapeutic Potential for Cancer Treatment. *J. Med. Chem.* **2017**, 60, 10205-10219. doi: 10.1021/acs.jmedchem.7b01520

16. Fodor, M.; Price, E.; Wang P.; Lu H.; Argintaru A.; Chen Z.; Glick M.; Hao H.; Kato, M.; Koenig, R.; LaRochelle, J.R.; Liu, G.; McNeill, E,; Majumdar, D.; Nishiguchi, G.A.; Perez, L.B.; Paris, G.; Quinn, C.M.; Ramsey, T.; Sendzik, M.; Shultz, M.D.; Williams, S.L.; Stams, T.; Blacklow, S.C.; Acker, M.G.; LaMarche M.J.; Dual Allosteric Inhibition of SHP2 Phosphatase. *ACS Chem. Biol*. **2018**, 13, 647-656. doi: 10.1021/acschembio.7b00980

17**.** Bagdanoff, J.T.; Chen, Z.; Acker, M.; Chen, Y.N.; Chan, H.; Dore, M.; Firestone, B.; Fodor, M.;Garcia-Fortanet, J.; Hentemann, M.; Kato, M.; Koenig, R.; LaBonte, L.R.; Liu, S.; Mohseni, M.; Ntaganda, R.; Sarver, P.; Smith, T.; Sendzik, M.; Stams, T.; Spence, S.; Towler, C.; Wang, H.; Wang, P.; Williams, S.L.; LaMarche, M.J. Optimization of Fused-Bicyclic Allosteric SHP2 Inhibitors. *J. Med. Chem*. **2018**, companion manuscript jm-2018-01725j to be published in same issue.

18. Gee, K. R.; Sun, W. C.; Bhalgat, M. K.; Upson, R. H.; Klaubert, D. H.; Latham, K. A.; Haugland, R. P. Fluorogenic Substrates Based on Fluorinated Umbelliferones for Continuous Assays of Phosphatases and Beta-Galactosidases. *Anal. Biochem.* **1999,** *273,* 41-48.

19. (a) Wenlock, M. C.; Austin, R. P.; Barton, P.; Davis, A. M.; Leeson, P. D. A Comparison of Physicochemical Property Profiles of Development and Marketed Oral Drugs. *J. Med. Chem.* **2003,** *46,* 1250-1256. (b) Leeson, P. D.; Springthorpe, B. The Influence of Drug-Like Concepts on Decision-Making in Medicinal Chemistry. *Nat. Rev. Drug. Disc.* **2007,** *6,* 881-890. (c) Shultz, M. D. Setting Expectations in Molecular Optimizations: Strengths and Limitations of Commonly Used Composite Parameters. *Bioorg. Med. Chem. Lett.* **2013,** *23,* 5980-5991.

20. Artursson, P.; Tavelin, S. Caco-2 and Emerging Alternatives for Prediction of Intestinal Drug Transport: A General Overview. *Methods Princ. Med. Chem.* **2003,** *18,* 72−82.

21. (a) Summa, V.; Petrocchi, A.; Bonelli, F.; Crescenzi, B.; Donghi, M.; Ferrara, M.; Fiore, F.; Gardelli, C.; Paz, O. G.; Hazuda, D. J.; Jones, P.; Kinzel, O.; Laufer, R.; Monteagudo, E.; Muraglia, E.; Nizi, E.; Orvieto, F.; Pace, P.; Pescatore, G.; Scarpelli, R.; Stillmock, K.; Witmer, M. V.; Rowley, M. Discovery of Raltegravir, a Potent, Selective Orally Bioavailable HIV-Integrase Inhibitor for the Treatment of HIV-AIDS Infection. *J. Med. Chem.* **2008,** *51,* 5843−5855. (b) Kennis, J.E.J.; Vandenberk, J. Novel 1,2-Benzisoxadol-3-yl and 1,2-Benzisothiazol-3-ylderivatives. US Patent 4,804,633, 1985. (c) Zhang, Z.; Wallace, M. B.; Feng, J.; Stafford, J. A.; Skene, R. J.; Shi, L.; Lee, B.; Aertgeerts, K.; Jennings, A.; Xu, R.; Kassel, D. B.; Kaldor, S. W.; Navre, M.; Webb, D. R.; Gwaltney II, S. L. Design and Synthesis of Primidinone and Pyrimidinedione Inhibitors of Dipeptidyl Peptidase IV. *J. Med. Chem.* **2011,** *54,* 510-524.

22. Chen, C.H.; Chen, Z.; Dore, M.; Fortanet, J.G.; Karki, R.; Kato, M.; LaMarche, M.J.; Perez, L.B.; Smith, T.D.; Williams, S.; Girlades, S.; Toure, B.B.; Sendzik, M. N-Azaspirocycloalkane

Substituted N-Heteroaryl Compounds and Compositions for Inhibiting the Activity of SHP2. WO15107495, 2015.

23. Bhalay, G.; Culshaw, A. J.; Dziadulewicz, E. K.; Brain, C. T.; Ritchie, T. J.; Beattie, D.; Bala, K. J.; Brewer, A.; Hughes, G. Organic Compounds. WO2007/065662 A2*,* 2007.

24. Gillis, E. P.; Eastman, K. J.; Hill, M. D.; Donnelly, D. J.; Meanwell, N. A. Applications of Fluorine in Medicinal Chemistry. *J. Med. Chem.* **2015,** *58,* 8315-8359.

25 Dose Finding Study of TNO155 in Adult Patients With Advanced Solid Tumors, ClinicalTrials.gov Identifier: NCT03114319.

26. Kabsch, W. XDS. *Acta Cryst.* **2010,** *D66*, 125-132.

27. Bricogne, G.; Blanc, E.; Brandl, M.; Flensburg, C.; Keller, P.; Paciorek, W.; Roversi, P.; Smart, O. S.; Vonrhein, C.; Womack, T. O. BUSTER, version 2.8.0; Global Phasing Ltd, Cambridge, United Kingdom, 2009.

28. Emsley, P.; Lohkamp, B.; Scott, W. G.; Cowtan, K. Features and Devlopment of Coot. Acta Crystallogr., Sect. D: Biol. Crystallogr. **2010**, *D66,* 486−501.